THE JOURNAL OF PHYSICAL CHEMISTRY C
A JOURNAL OF THE AMERICAN CHEMICAL SOCIETY

pubs.acs.org/JPCC

Article

CO Adsorption and Disproportionation on Smooth and Defect-Rich Ir(111)

Xia Li, Thomas Haunold, Stefan Werkovits, Laurence D. Marks, Peter Blaha, and Günther Rupprechter*

Cite This: J. Phys. Chem. C 2022, 126, 6578−6589

Read Online

ACCESS | Metrics & More | Article Recommendations | Supporting Information

ABSTRACT: CO adsorption and dissociation on "perfect" and "defect-rich" Ir(111) surfaces were studied by a combination of surface-analytical techniques, including polarization-dependent (PPP and SSP) sum frequency generation (SFG) vibrational spectroscopy, low-energy electron diffraction (LEED), Auger electron spectroscopy, X-ray photoelectron spectroscopy (XPS), and density functional theory (DFT) calculations. CO was found to be ordered and tilted from the surface normal at high coverage on the "perfect" surface (e.g., θ = 30° at 0.70 ML), whereas it was less ordered and preferentially upright (θ = 4−10°) on the "defect-rich" surface for coverages of 0.55−0.70 ML. SFG, LEED, and XPS revealed that CO adsorption at low pressure/high temperature and high pressure/low temperature was reversible. In contrast, upon heating to ∼600 K in near mbar CO pressure, "perfect" and even more "defect-rich" Ir(111) surfaces were irreversibly modified by carbon deposits, which, according to DFT, result from CO disproportionation.

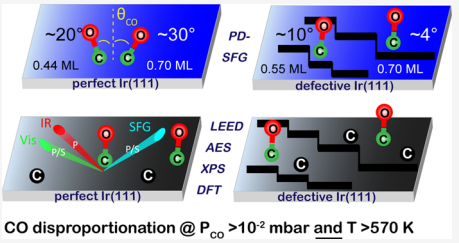

1. INTRODUCTION

Iridium surfaces have repeatedly attracted interest due to their thermo-catalytic properties.[1−4] Iridium is also used in electro- and photocatalysis, employing Ir, Ir alloys (e.g., PtIr, RuIr, and PtNiIr), and IrO_2 as nanoparticles or thin films.[5−10] Previous surface science studies have shown that the Ir(100) surface may undergo a (1 × 1) → (5 × 1) surface reconstruction, which was lifted by the adsorption of small molecules (e.g., CO).[11−15] Ir(110) also shows a (1 × 2) missing-row-type reconstruction with (111) micro-facets,[16] while Ir(111) is reported to be the most stable surface.[17]

CO adsorption on Ir(111) has been studied for over 50 years by experimental surface science techniques such as low-energy electron diffraction (LEED), Auger electron spectroscopy (AES), temperature-programmed desorption (TPD), Fourier transform infrared reflection-adsorption spectroscopy (FT-IRAS), X-ray photoelectron spectroscopy (XPS), and sum frequency generation (SFG) spectroscopy,[1,4,18−26] as well as by density functional theory (DFT).[24,27,28] Two distinct LEED patterns indicated an ordered $(\sqrt{3} \times \sqrt{3})R30°$ structure at 1/3 ML[1,17−19] and a (diffuse) $(2\sqrt{3} \times 2\sqrt{3})R30°$ pattern at high coverage (7/12 ML[19] and 2/3 ML[1,18]). With increasing CO coverage, FT-IRAS showed that the IR spectral intensities of linearly (on-top) bonded CO increased and vibrational frequencies blue-shifted,[20,24] while in TPD, the desorption peaks shifted to lower temperature and different adsorption states formed, especially close to saturation.[18−20] Such observations/trends are quite common for CO adsorption on metals, but we could recently demonstrate that upon increasing the coverage, CO was tilted on Ir(111) [at 0.77 ML by about 20° (DFT) or 36° (SFG)].[25] Apparently, the CO adsorbate structures are strongly coverage-dependent, same as for Pd(111) surfaces (although CO populates hollow or bridge in addition to on-top sites on Pd).[29−32]

Herein, we reveal the effect of surface roughness on CO adsorption by extending the picture to "defect-rich" (sputtered) Ir(111) surfaces. Whereas conventional vibrational spectroscopy would detect only minor frequency shifts, polarization-dependent (PD-) SFG enables us to directly monitor the effect of defects on the molecular arrangement and orientation of the CO overlayer. SFG spectroscopy was carried out at a "near ambient pressure" of 1 mbar and at temperatures up to 600 K, which induced irreversible surface changes, likely originating from CO dissociation. Carbon deposits were detected by AES, and the reaction pathway via CO disproportionation was examined by DFT.

2. METHODS

2.1. Basic Theory of Polarization-Dependent SFG. IR−visible SFG is a second-order surface-specific process as the effective second-order nonlinear susceptibility $\chi^{(2)}_{eff} \neq 0$ at an anisotropic surface/interface. Polarization-dependent SFG spectra of adsorbed molecules are usually taken with PPP and SSP polarizations (the indices are defined in the order of SFG, visible and IR beams), which allows a quantitative analysis of

Received: February 16, 2022
Revised: March 26, 2022
Published: April 8, 2022

https://doi.org/10.1021/acs.jpcc.2c01141
J. Phys. Chem. C 2022, 126, 6578−6589

molecular orientation.[25,33−39] The SFG spectra can be fitted by Lorentzian lineshapes:

$$I_{SFG} \propto |\chi^{(2)}_{eff}|^2 = \left| \chi^{(2)}_{NR} + \sum \frac{\chi^{(2)}_{eff,q}}{\omega_{IR} - \omega_q + i\Gamma_q} \right|^2 \quad (1)$$

where $\chi^{(2)}_{NR}$ is the magnitude of the non-resonant susceptibility generated by the substrate. χ_q, ω_q, and Γ_q represent the resonance amplitude, frequency, and damping constant of the qth vibrational mode, respectively. When ω_{IR} is close or equal to ω_q, the SFG intensity (i.e., I_{SFG}) is enhanced and a vibrational peak appears in the SFG spectrum. The interfacial molecular orientations can be determined in an SFG experiment because the measured $\chi^{(2)}_{eff}$ is related to the macroscopic second-order susceptibility in the laboratory coordinates ($\chi^{(2)}_{ijk}$) by

$$\chi^{(2)}_{eff} = [e(\omega_{SFG})\cdot\boldsymbol{L}(\omega_{SFG})]\cdot\chi^{(2)}_{ijk}\vdots [e(\omega_{Vis})\cdot\boldsymbol{L}(\omega_{Vis})] [e(\omega_{IR})\cdot\boldsymbol{L}(\omega_{IR})] \quad (2)$$

where $e(\omega_i)$ refers to the unit electric field vector and $\boldsymbol{L}(\omega_i)$ is the Fresnel factor determined by the laser incidence and refraction angles, polarizations, and refractive indices.[33,34,36,40] Furthermore, $\chi^{(2)}_{ijk}$ is related to the microscopic hyperpolarizability tensor elements $\beta^{(2)}_{i'j'k'}$ in the molecular coordinate system through Euler transformation $\langle R_{ii'}R_{jj'}R_{kk'}\rangle$ by[41]

$$\chi^{(2)}_{ijk} = N_s \sum_{i'j'k'} \langle R_{ii'}R_{jj'}R_{kk'}\rangle \beta^{(2)}_{i'j'k'} \quad (3)$$

Here, N_s is the effective molecular surface number density per unit. For CO with $C_{\infty v}$ symmetry, the molecules have a random azimuthal distribution, and the surface CO orientation (tilt angle θ, the CO molecular axis with respect to the surface normal) can be determined by measuring I_{PPP}/I_{SSP} for a known molecular hyperpolarizability ratio R (i.e., $R = \beta^{(2)}_{aac}/\beta^{(2)}_{ccc} = \beta^{(2)}_{bbc}/\beta^{(2)}_{ccc}$), assuming a δ-function for the orientation distribution.[25,42]

2.2. UHV Preparation/Analysis Chamber Coupled to a UHV-High-Pressure Cell for SFG Spectroscopy. All LEED/AES and SFG experiments were carried out in a custom-designed ultrahigh-vacuum (UHV) preparation/analysis chamber coupled to a UHV-to-atmospheric pressure-compatible SFG spectroscopic cell. The experimental setup has been described in detail previously.[43]

2.2.1. UHV Preparation/Analysis Chamber Equipped with LEED/AES Optics. The UHV chamber is a stainless-steel vessel of about 40 L, which is pumped to a routine base pressure of 5 × 10^{-10} mbar by a turbomolecular drag pump Pfeiffer TMU, monitored by a hot-cathode gauge (Leybold IONIVAC ITR 90, GRAPHIX ONE controller). The chamber is further equipped with a four-grid retractable LEED/AES optics (SPECS ErLEED DN 150 CF) and a 3000D controller with a thoria (ThO_2)-coated Ir filament that allows for a maximum of 10^{-6} mbar operation pressure. LEED patterns are recorded using a CMOS-sensor camera. The ErLEED 3000D power supply provides all necessary voltages to operate a LEED optics as a retarding field analyzer (RFA) for AES. For recording AES data, an integrated lock-in amplifier and RFC-PC software are used.

The Ir(111) single crystal was disk-shaped, with 8 mm diameter and 2 mm thickness. For a smooth/"perfect" surface, Ir(111) was pretreated by repeated cycles of sputtering with Ar^+ ions (beam energy 1.2 keV at 5 × 10^{-6} mbar Ar, 30 min), oxidation (1 × 10^{-7} mbar O_2, 30 min) at 800 K, and UHV annealing at 1050 K for 30 min, as described in refs 15, 18, 44, 45. This leads to ordered and clean surfaces, as confirmed by and described in detail in ref 15. LEED and AES were employed to verify the long-range order and cleanliness of the surface, respectively. For the sputtered "defect-rich" surface, freshly prepared "perfect" Ir(111) was sputtered with Ar^+ ions using a beam energy of 1.2 keV at 5x10^{-6} mbar Ar for 40 min at 300 K (without subsequent annealing). For scanning tunneling microscopy (STM) images of a sputtered single crystal surface with three-dimensional islands exhibiting a very high density of steps and edges, one should refer to ref 46. CO of purity 4.7 (99.997%) from Messer Austria was used, further passed through a cold trap (AES confirmed that no Ni or Fe impurities were present[47]), with the CO overlayer structures characterized by LEED.

2.2.2. UHV-High-Pressure Cell for SFG Spectroscopy. The freshly pretreated Ir(111) can be directly transferred from the UHV chamber to the SFG cell under UHV, avoiding contaminations. The SFG cell can be operated from 2.5 × 10^{-8} mbar to 1 bar pressure and at 100−800 K. SFG measurements were performed using a 20 ps mode-locked Nd:YAG laser system (EKSPLA, PL2241) with a fundamental radiation of 1064 nm (30 mJ/pulse, 50 Hz repetition rate). A tunable mid-infrared beam (with the photon energy ω_{IR}) and a visible beam with a fixed wavelength of 532 nm were directed in a co-propagation geometry toward the Ir(111) surface (for details, see refs 39, 42, 43), with incidence angles of 55° and 58.5° with respect to the surface normal, respectively. The pulse energy was 90−130 μJ for infrared between 1850 and 2150 cm^{-1} and 30 ± 5 μJ for visible. The SFG signal was collected/detected in the reflection direction with a photomultiplier tube (PMT). The polarization of IR was kept as P and that of visible and SFG signal was switched between P and S using a Glan−Taylor prism and a half-wave plate. All spectra were normalized by the energy of visible and IR laser pulses and fitted using Lorentzian lineshapes (eq 1).

2.3. X-ray Photoelectron Spectroscopy. XPS experiments were carried out in another stainless-steel UHV chamber (35 L, base pressure < 5 × 10^{-10} mbar). A SPECS XR50 high-intensity nonmonochromatic Al/Mg dual-anode X-ray source and a Phoibos 100 hemispherical energy analyzer (EA) with a multichannel plate detector were used for XPS, as described in ref 48. Al K_α radiation (1486.61 eV) was used for the acquisition of XPS spectra. In this chamber, the sample preparation and surface order analysis by LEED followed the same procedure as described above.

2.4. Density Functional Theory. The disproportionation of two CO molecules on the Ir(111) surface into CO_2 and C was studied by DFT using the augmented plane wave and local orbital (APW + lo) method as implemented in our WIEN2k code.[49,50] The calculations of the present work used the generalized gradient approximation by Perdew, Burke, and Ernzerhof (PBE).[51,52] We used a plane wave cutoff parameter $R_{MT}K_{max}$ = 5 for all calculations with a C atom and a properly scaled $R_{MT}K_{max}$ for the pure Ir surface, where R_{MT} refers to the smallest atomic sphere radius (2.2/1.05/0.95 bohr for Ir, O, and C atomic spheres, respectively). The final results were checked with $R_{MT}K_{max}$ = 6. A 4 × 4 × 1 (checked with 8 × 8 × 1) k-mesh was used, and the self-consistent field calculations and the atomic positions were fully relaxed until the forces were smaller than 1 mRy/bohr.

https://doi.org/10.1021/acs.jpcc.2c01141
J. Phys. Chem. C 2022, 126, 6578−6589

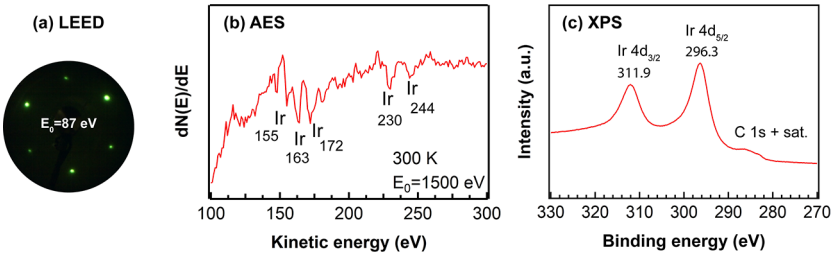

Figure 1. Characterization of clean Ir(111) at 300 K in UHV: (a) LEED pattern at E_0 = 87 eV; (b) AES spectrum at E_0 = 1500 eV; and (c) Ir 4d + C 1s region XPS spectrum.

3. RESULTS AND DISCUSSION

3.1. Surface Characterization of Clean Ir(111) by LEED, AES, and XPS. Before CO adsorption, an ordered and clean Ir(111) was confirmed by LEED, AES, and XPS. As shown in Figure 1a, a hexagonal LEED pattern with sharp spots on a low background indicated a well-ordered Ir(111) surface. In AES spectra (Figure 1b), five Ir peaks in the absence of a carbon peak (expected around 272 eV[18,53]) demonstrated a clean surface. Unfortunately, the XPS C 1s analysis of C species on clean Ir(111) was somewhat hindered by overlapping satellite features of the Ir 4d peak due to the use of a nonmonochromatized X-ray source.[15] As shown in Figure 1c, Al $K_{\alpha 3}$ and $K_{\alpha 4}$ satellites (at binding energies of 286.5 and 284.5 eV, respectively) of Ir $4d_{5/2}$ (at a binding energy of 296.3 eV) overlapped with the C 1s region. Still, significant amounts of carbon can be excluded.

3.2. LEED Patterns of CO Adsorption on Clean and Smooth Ir(111). Previous LEED studies of CO on Ir(111) reported that $(\sqrt{3} \times \sqrt{3})R30°$ and $(2\sqrt{3} \times 2\sqrt{3})R30°$ overlayer structures typically formed under UHV conditions.[19] However, in the (>1.0) mbar regime, a more complex $(3\sqrt{3} \times 3\sqrt{3})R30°$ structure forms instead.[44,54] Our observations are consistent with these results.

As shown in Figures 2 and S1, on the clean Ir(111) surface, a (1 × 1) LEED pattern formed, whereas upon CO

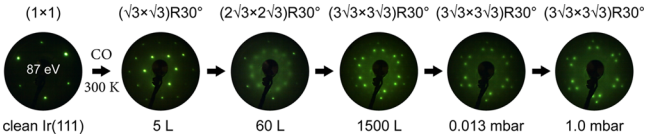

Figure 2. Evolution of LEED patterns at E_0 = 87 eV of CO overlayer structures on Ir(111) as a function of CO exposure at 300 K: 5 and 60 L (1 Langmuir ≈ 10^{-6} mbar·s) were obtained by dosing CO at 5 × 10^{-8} mbar for 100 and 1200 s, respectively, and 1500 L was achieved by dosing CO at 5 × 10^{-7} mbar for 50 min. Pressures of 10^{-2} to 1 mbar were applied in the high-pressure SFG cell, with LEED taken after pump-down and transfer.

chemisorption at 300 K and at 5 × 10^{-8} mbar pressure, $(\sqrt{3} \times \sqrt{3})R30°$ and $(2\sqrt{3} \times 2\sqrt{3})R30°$ patterns were observed after 5 and 60 L exposure, respectively. When Ir(111) was exposed to 1500 L of CO (at 5 × 10^{-7} mbar), a $(3\sqrt{3} \times 3\sqrt{3})R30°$ pattern was present.[44,54] Further increasing the CO pressure to 1.0 mbar maintained the $(3\sqrt{3} \times 3\sqrt{3})R30°$ overlayer structure. Accordingly, a CO-$(3\sqrt{3} \times 3\sqrt{3})R30°$ structure is formed not only at mbar pressure but also upon high exposure at relatively low pressure.

3.3. SFG Spectra of CO Adsorption on Ir(111): The "Perfect" vs "Defect-Rich" Surface. *3.3.1. Pressure-Dependent PPP and SSP Spectra.* Figure 3 compares the pressure-dependent SFG spectra of CO on the "perfect" and "defect-rich" Ir(111) surfaces at 300 K, in the range of 10^{-7} to 1 mbar, both for PPP and SSP polarization combinations. A previous combined IRAS/TPD study of CO/Ir(111) deduced a relationship between the IR peak position and the CO coverage,[20] which is utilized herein to convert SFG peak positions to coverages for both surfaces as the differences in peak positions are small. Still, the coverages on the "defect-rich" surface may be slightly underestimated. In the 10^{-6} mbar range, the observed peak positions are well in line with IRAS studies of CO on Ir(111) and graphene-supported Ir clusters.[24]

A single peak, characteristic of on-top CO, was observed on both surfaces. As pressure increased from 10^{-7} to 1.0 mbar, the CO vibrational frequency moved from 2084 to 2094 cm^{-1} (coverage 0.62 to 0.77 ML) and from 2079 to 2090 cm^{-1} (coverage 0.56 to 0.70 ML) on "perfect" (Figure 3a,b) and "defect-rich" Ir(111) (Figure 3c,d), respectively. The frequency blue shifts can be attributed to the increasing dipole−dipole coupling and chemical shift.[20,55−57] On the defective surface, the observed wavenumber is typically ∼5 cm^{-1} lower than on the smooth surface under the same conditions, reflecting the low-coordinated sites. Furthermore, in Figure 3c,d, assuming a second peak (<2080 cm^{-1}), representing CO adsorbed on defects (e.g., steps, kinks, adatoms, and vacancies),[39,58−60] was required to fit the experimental spectra (Figure S2). Accordingly, the full width at half-maximum (FWHM = 2Γ) of the on-top CO peak was 4 cm^{-1} larger (∼12 vs ∼8 cm^{-1}) as the CO layer was less homogeneous on "defect-rich" surfaces.

For both surfaces, the CO peak positions acquired from PPP and SSP spectra were nearly identical (Figure 3e), but the spectral intensities (i.e., I_{PPP} and I_{SSP}) exhibited different trends with increasing coverage/pressure: for CO on "perfect" Ir(111), I_{PPP} decreased, but I_{SSP} increased, whereas for CO on "defect-rich" Ir(111), both I_{PPP} and I_{SSP} hardly changed but overall decreased. Above 10^{-3} mbar, both vibrational frequency and intensity changed moderately because saturation was nearly reached. The fitting results of CO on "perfect" and "defect-rich" Ir(111) can be found in ref 25 and Table S1, respectively.

Our recent work about CO on smooth Ir(111) had pointed out that a decreasing I_{PPP} and an increasing I_{SSP} (Figure 3a,b,f) (smaller I_{PPP}/I_{SSP}) indicate an increasing tilt angle (θ), with θ increasing from 25° to 36° as the coverage increased from 0.62 to 0.77 ML.[25] As CO tilted closer to the surface (i.e., larger θ), it yielded a relatively strong SSP signal (thus having a good signal-to-noise ratio) but caused a drop in the PPP signal. For CO on "defect" Ir(111), SSP shows a poor signal-to-noise ratio

https://doi.org/10.1021/acs.jpcc.2c01141
J. Phys. Chem. C 2022, 126, 6578−6589

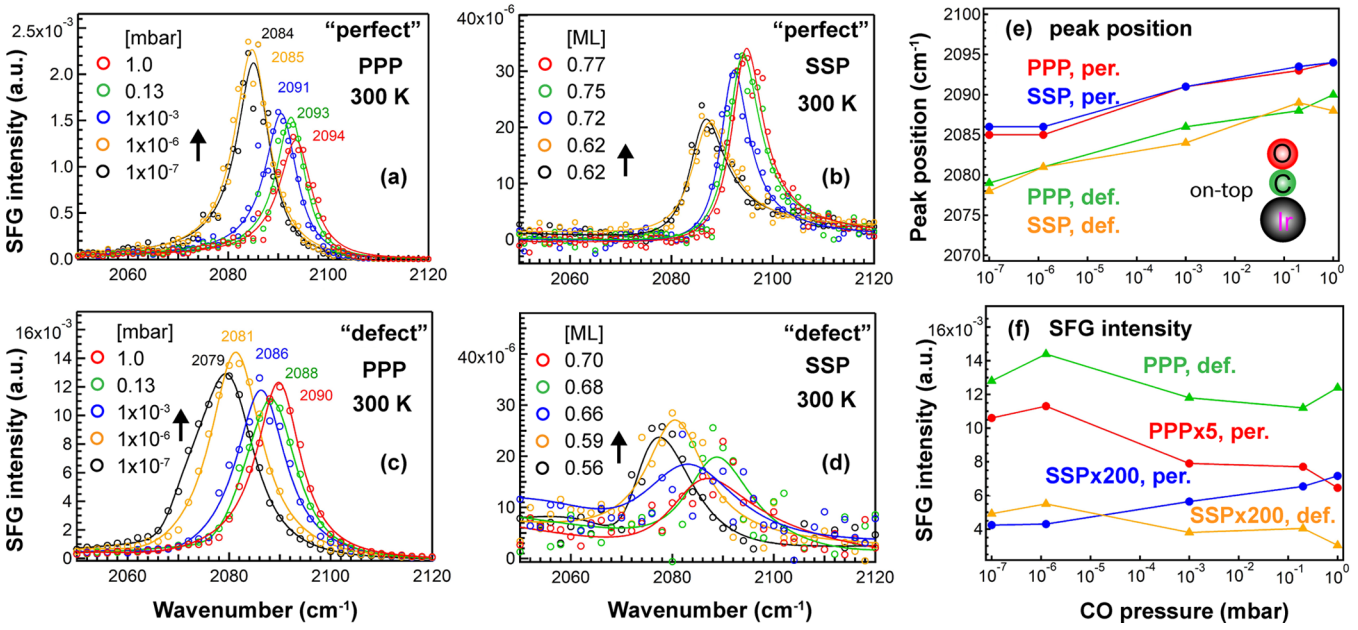

Figure 3. Pressure-dependent (10^{-7} to 1 mbar) SFG spectra of on-top CO on "perfect" and "defect-rich" Ir(111) at 300 K: (a,c) PPP and (b,d) SSP. All PPP and SSP peak positions and spectral intensities as a function of CO pressure are summarized in (e,f), respectively. Adapted in part with permission from ref 25. Copyright 2020 American Chemical Society.

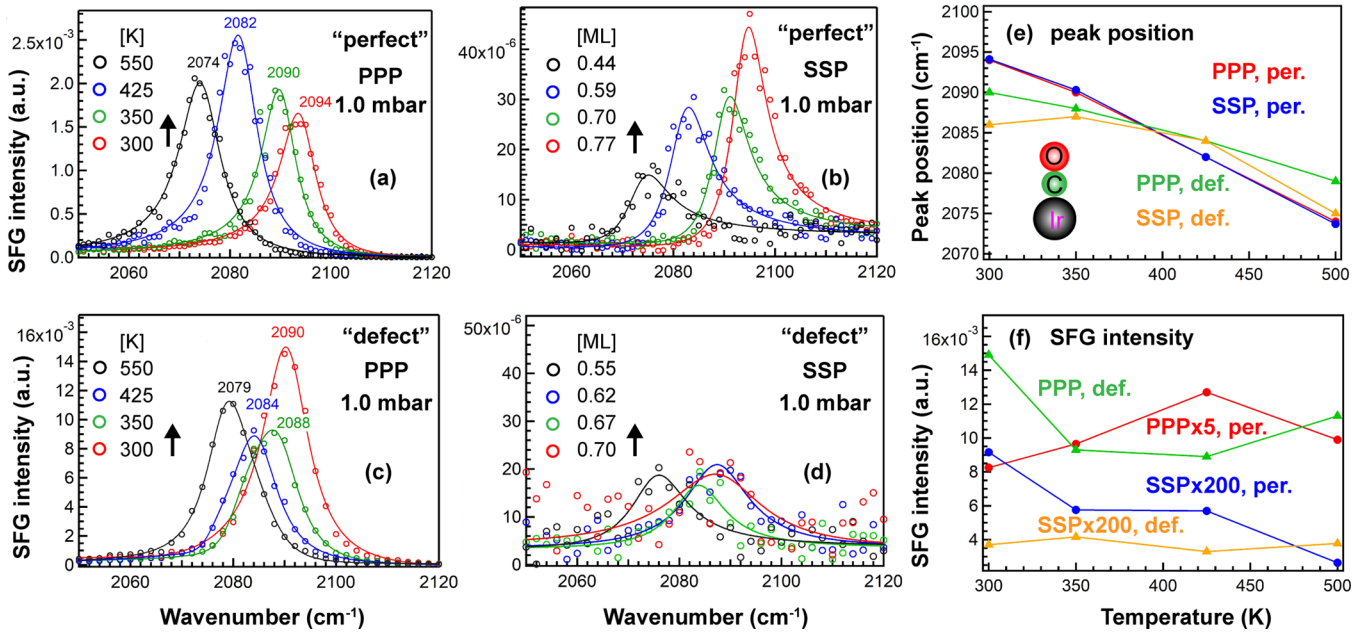

Figure 4. Temperature-dependent (300−500 K) SFG spectra of 1 mbar CO on "perfect" and "defect-rich" Ir(111): (a,c) PPP and (b,d) SSP. All PPP and SSP peak positions and spectral intensities as a function of substrate temperature are summarized in (e,f), respectively. Adapted in part with permission from ref 25. Copyright 2020 American Chemical Society.

and is mostly due to the non-resonant background, whereas PPP was strong. Overall, this indicates a small θ so that CO is upright on defective Ir(111). I_{PPP} on the defective surface was stronger than on the perfect surface, likely due to a combined effect of the CO tilt angle, order, and coverage.

3.3.2. Temperature-Dependent PPP and SSP Spectra. SFG spectra were also acquired for both types of surfaces upon varying (lowering) the CO coverage by increasing the surface temperature from 300 to 500 K in a constant background of 1 mbar CO (Figure 4). As the temperature increased, the CO frequency red-shifted to low wavenumbers because of decreasing dipole coupling and different chemical shifts. Interestingly, the red shift on the defective surface was smaller than that on the smooth surface (11 vs 20 cm^{-1}, respectively), which points to a smaller coverage change on the "defect-rich" surface that binds CO stronger. The fitting results of CO on the "perfect" and "defect-rich" Ir(111) can be found in ref 25 and Table S1, respectively.

As previously reported in detail for CO/"perfect" Ir(111), upon temperature increase, PPP and SSP changed oppositely (Figure 4a,b,f); that is, I_{PPP} first increased and then decreased, while I_{SSP} decreased gradually. The CO tilt angle decreased

https://doi.org/10.1021/acs.jpcc.2c01141
J. Phys. Chem. C 2022, 126, 6578−6589

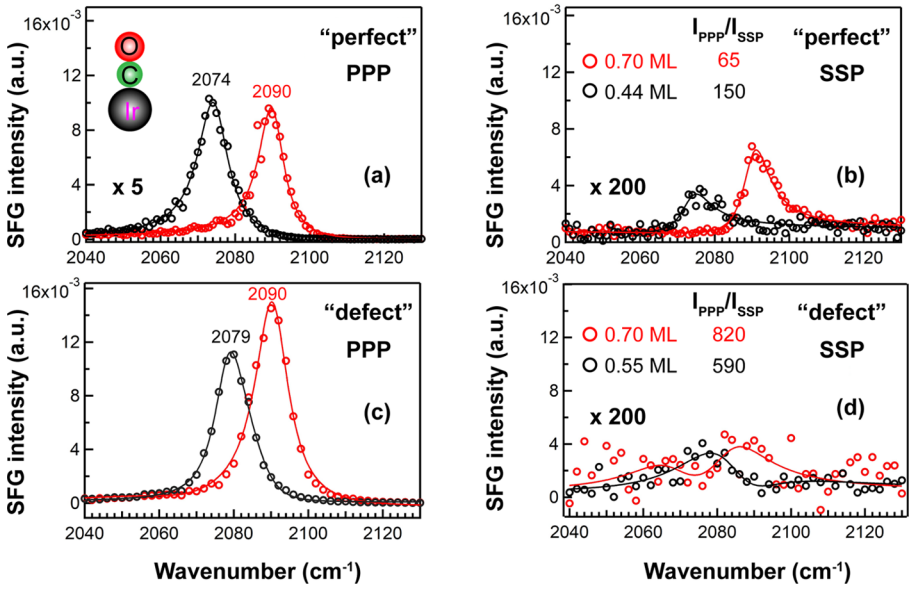

Figure 5. Selected SFG spectra of CO on "perfect" and "defect-rich" Ir(111): (a,c) PPP and (b,d) SSP.

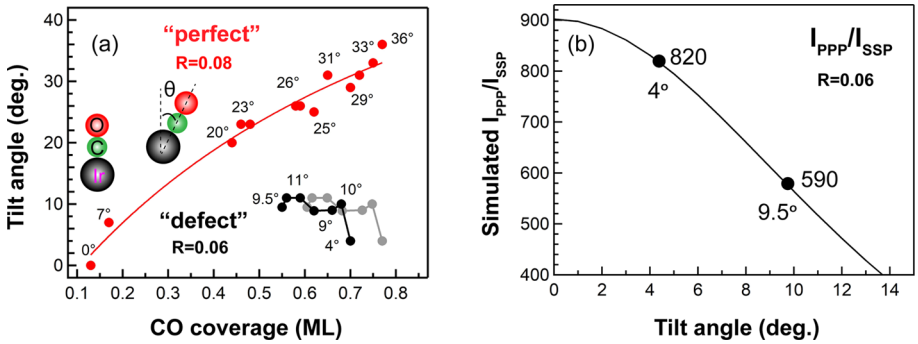

Figure 6. (a) Tilt angle (θ) of CO as a function of coverage, both for "perfect" and "defect-rich" Ir(111). The gray dots illustrate that the coverage on "defect-rich" may be slightly larger. (b) Simulated I_{PPP}/I_{SSP} for CO/Ir(111) as a function of θ for a CO hyperpolarizability ratio R = 0.06. For parameters used in the simulations, one should refer to ref 25. Adapted in part with permission from ref 25. Copyright 2020 American Chemical Society.

from 36° to 20° when the coverage decreased from 0.77 to 0.44 ML,[25] so the increase of I_{PPP} was mainly attributed to a decreasing θ, and the decreasing I_{SSP} was due to the decreasing coverage and decreasing θ. In contrast, for CO on "defect-rich" Ir(111), PPP obviously decreased, whereas SSP changed only slightly. Similar to Figure 3, I_{PPP} was larger and I_{SSP} was smaller, once more confirming a small tilt angle θ on the defective surface.

3.3.3. Quantitative Analysis of the CO Tilt Angle on Ir(111): "Perfect" vs "Defect-Rich". In order to illustrate that the CO tilt angle on the "perfect" and "defect-rich" surfaces exhibited different coverage dependences, the PPP and SSP spectra were compared at two similar coverages, as shown in Figure 5. Notably, polarization-dependent SFG reveals a striking difference: for smooth Ir upon increasing the coverage (0.44 to 0.70 ML) (Figure 5a,b), I_{PPP} slightly decreased and I_{SSP} obviously increased. In contrast, for the defective Ir surface, I_{PPP} was distinctively larger and I_{SSP} was moderately larger at higher coverage (Figure 5c,d). This already illustrates a different trend.

As mentioned, the CO tilt angle can be deduced from I_{PPP}/I_{SSP} if the R-value is known.[25,39] Using CO on smooth Ir(111)[25] at 0.13 ML (upright CO, θ = 0°) with I_{PPP}/I_{SSP} = 520 as the reference, R was determined to be 0.08. Accordingly, for CO/"perfect" Ir(111),[25] I_{PPP}/I_{SSP} of 150 and 65 at 0.44 and 0.70 ML coverage (Figure 5a,b) indicates corresponding tilt angles of 20° and 30°, respectively (Figure 6a). Indeed, DFT calculations of the potential energy surface as a function of tilt angle for two CO molecules in nearest-neighbor positions in a 3 × 3 Ir(111) supercell had indicated that the energy increased dramatically when CO molecules came closer.[25] Only when the CO molecules bent to the same direction ("concerted tilting"), the curve became flat.

For CO on "defect-rich" Ir(111), I_{PPP}/I_{SSP} was 820 at 0.70 ML coverage (Figure 5c,d), and no reasonable θ can thus be obtained with R = 0.08. However, our recent work already reported the simulated I_{PPP}/I_{SSP} versus θ for different R values (0.08, 0.07, and 0.06).[25] With R decreased to 0.07 and 0.06, the maximum of I_{PPP}/I_{SSP} increased to 670 and 900, respectively. Therefore, using R = 0.06 for 0.70 ML CO on the defective Ir(111), θ was determined to be 4° (Figure 6b). For 0.55 ML CO on defective Ir, I_{PPP}/I_{SSP} was 590 pointing to a θ of 9.5°, that is, a somewhat higher tilt angle at lower coverage (opposite the trend on perfect Ir). Table S1 summarizes all tilt angles at different coverages for CO on "defect-rich" Ir(111) (based on the pressure- and temperature-

https://doi.org/10.1021/acs.jpcc.2c01141
J. Phys. Chem. C 2022, 126, 6578−6589

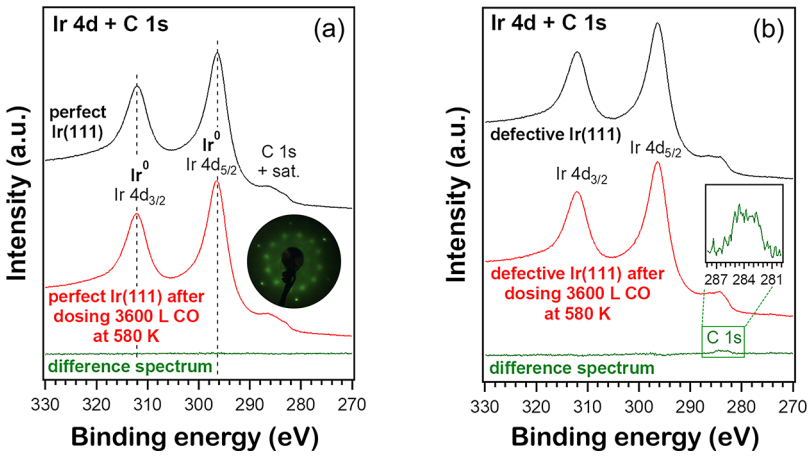

Figure 7. (a) Ir 4d + C 1s XPS spectra of perfect Ir (111) before and after annealing in 1×10^{-6} mbar CO at 580 K for 60 min, followed by cooling in UHV (spectra acquired at room temperature). The inset shows the subsequently acquired LEED pattern after dosing 300 L of CO at 300 K. (b) Corresponding Ir 4d + C 1s XPS spectra of defective Ir(111) before and after the same annealing as in (a).

dependent spectra in Figures 3 and 4). Except for $\theta = 4°$ at 0.70 ML, θ was ~10° at all other coverages (0.67−0.55 ML, $R = 0.06$) (Figure 6a).

Summarizing the adsorption studies of CO on "defect-rich" Ir(111), the CO tilt angle was found to be small (4−10°) with only weak coverage depencence. The SFG spectral changes were mainly due to coverage changes. On the defective rough surface, the CO molecules seem to form a less-ordered overlayer and neighboring CO molecules are frequently located in different planes. This reduces the dipole−dipole repulsion so that "concerted tilting" is not induced and θ remains small. In summary, the surface roughness removed the strong coverage dependence of the CO tilt angle, observed on smooth Ir(111), so that on a rough surface CO was overall quite upright.

3.4. XPS, LEED, SFG, and AES Studies of CO Dissociation. DFT calculations have shown that CO cannot dissociate on Ir(111) due to a high effective barrier of 3.17 eV.[28] This agrees with an ultraviolet photoelectron spectroscopy (UPS) study of Ir(111) in 10^{-8} Torr CO, which demonstrated that CO does not dissociate at an appreciable rate at 533 K.[61] However, it was reported that heating Ir(111) to ≥650 K in $\geq 10^{-6}$ mbar CO[19] or to ≥773 K in $\geq 10^{-8}$ mbar CO[18] may result in significant dissociation. Therefore, in the following, a possible CO dissociation is examined for three different combinations of pressure and temperature by various surface-sensitive techniques: (i) XPS/LEED at low pressure, high temperature; (ii) SFG at high pressure, low temperature; and (iii) SFG/AES (post-reaction) at high pressure, high temperature.

3.4.1. CO Dissociation at Low Pressure and High Temperature: XPS (10^{-6} mbar, 580 K) and LEED (10^{-5} mbar, 890 K). First, Ir 4d + C1s XPS spectra of "perfect" Ir(111) were acquired before and after dosing 3600 L of CO (10^{-6} mbar CO for 3600 s) at 580 K (Figure 7a). The flat difference spectrum reveals that CO does not dissociate on Ir(111) under these conditions. After cooling to 300 K in UHV and dosing 300 L of CO, the $(2\sqrt{3} \times 2\sqrt{3})R30°$-CO LEED pattern (Figure 7a, inset) verified the absence of CO dissociation. When the same experiment was repeated on defective Ir(111), only a very small amount of carbon was indicated by a tiny C 1s peak in the difference spectrum (Figure 7b).

Upon increasing the pressure to 10^{-5} mbar (for 60 min) and the temperature to 890 K (Figure 8), LEED showed complete

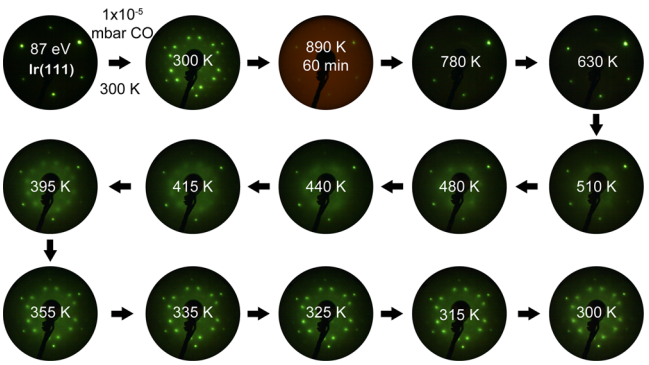

Figure 8. Evolution of LEED patterns at $E_0 = 87$ eV of CO overlayer structures on "perfect" Ir(111) upon annealing in 1×10^{-5} mbar CO at 890 K for 60 min and stepwise cooling to 300 K.

CO desorption on perfect Ir(111) as the $(3\sqrt{3} \times 3\sqrt{3})R30°$ -CO pattern disappeared and (1×1)-Ir(111) appeared. The red background of the LEED pattern originated from glowing Ta-wires. Upon subsequent cooling to 630 K at 10^{-5} mbar, no CO chemisorption was observed. CO started to adsorb on the surface at 510 K forming a rather diffuse $(\sqrt{3} \times \sqrt{3})R30°$ structure until relatively sharp spots appeared at 480 K. At 415 K, a $(2\sqrt{3} \times 2\sqrt{3})R30°$ structure began to develop. When the temperature was decreased from 355 to 300 K, $(3\sqrt{3} \times 3\sqrt{3})R30°$ occurred, reestablishing the pattern at 300 K before heating. Therefore, the reversible LEED patterns before and after heating to 890 K in 10^{-5} mbar CO also indicate that CO does not dissociate upon the combination of low pressure and high temperature. No meaningful LEED patterns can be observed on the sputtered surface, preventing a comparison.

3.4.2. SFG Study of CO Dissociation at High Pressure (1.0 mbar) and (Relatively) Low Temperature (500 K). When the Ir surfaces were stepwise heated in 1 mbar CO from 300 to 500 K, the SFG spectra acquired upon heating and cooling were identical; that is, the spectra were fully reversible (Figure 9). This suggests that the surface does not change; that is, CO dissociation was absent.

https://doi.org/10.1021/acs.jpcc.2c01141
J. Phys. Chem. C 2022, 126, 6578−6589

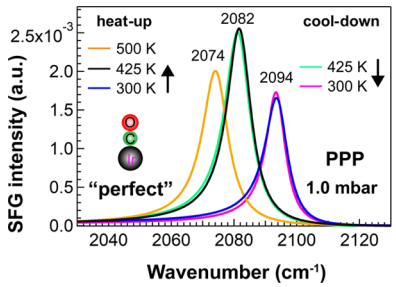

Figure 9. Selected PPP spectra of CO on "perfect" Ir(111) upon heating to 500 K and cooling in 1.0 mbar CO. For clarity, only the fitted lines are shown.

3.4.3. SFG Study of CO Dissociation at High Pressure (≥10^{-2} mbar) and (Relatively) High Temperature (≥575 K). Interestingly, when the substrate temperature reached 575 K, the SFG spectra acquired during heat-up were still "as-expected" (Figure 10a,b), whereas the spectra taken during cool-down were very different from the previous ones under the same nominal conditions; that is, there were irreversible changes in the spectra.

Figure 10 again compares smooth and "defect-rich" Ir(111) upon heat-up and cool-down. When comparing SFG PPP spectra of CO on "perfect" Ir(111) before and after reaching 575 K, it is apparent that (Figure 10a,b,e,f) (i) the vibrational frequencies were lowered by about 23 cm^{-1}, (ii) the spectral intensities were at least three times smaller (Table S2), and (iii) the spectral lineshapes became (more) asymmetric. All features indicate a strong modification of the Ir(111) surface, once reaching 575 K in 1.3 × 10^{-2} mbar CO. Strong restructuring of Ir(111) and/or CO dissociation may be responsible for the observed effect. Similar results were also found in an SFG study of CO adsorption and dissociation on Pt(111).[62,62] When Pt(111) was heated in 400 Torr CO to 823 K and then cooled to room temperature, an apparent hysteresis in CO vibrational frequency and a decrease in intensity were observed due to carbon formation at high temperature. The AES spectra of the Pt(111) surface after exposure to 400 Torr of CO at 673 K showed a notable carbon peak, also indicating CO dissociation on Pt(111) at this temperature.[62,63] For Pt thin films and nanoparticles in 10 mbar CO, dissociation was observed by SFG and near ambient pressure (NAP-)XPS upon heating to 550 K.[64] On smooth and sputtered Pd(111), no indications of CO dissociation were observed even after hours in 0.1 mbar CO, likely due to the temperature limit of 400 K.[65−67] It is well documented that carbon perturbs the electronic and geometric structure of stepped surfaces, which leads to poisoning.[68,69]

Upon cool-down (Figure 10b), the peak positions indicated a coverage increase from 0.1 to 0.29 ML, but the spectral intensities remained nearly unchanged. Based on our former work showing that CO was tilted at high coverage,[25] the expected increase in PPP intensity due to increasing coverage seems compensated by the loss of intensity due to an increasing tilt angle. Unfortunately, the SSP signals were too weak for detection after heating because even before heating I_{SSP} was >35 times smaller than I_{PPP}[25] (and after heating even I_{PPP} decreased three times).

The spectral reversibility was also investigated for the "defect-rich" Ir(111) surface. Figure 10c,d shows the PPP spectra before and after heating to 600 K at 1.0 mbar CO. Analogous to the smooth surface, after reaching 600 K, the spectra showed a red shift of about 13 cm^{-1} and the lineshapes changed to asymmetric. Note that the intensities were reduced even ∼20 times. Apparently, although similar in tendency, the changes were much stronger for the defect-rich surface, which may result from the roughness and/or the higher CO pressure (this will be further discussed below).

For CO/Ir(111), previous AES studies reported significant CO dissociation at >773 K at 10^{-8} mbar[18] or at ≥650 K at 1.33 × 10^{-6} mbar.[19] Accordingly, at 10^{-2} to 1.0 mbar CO used

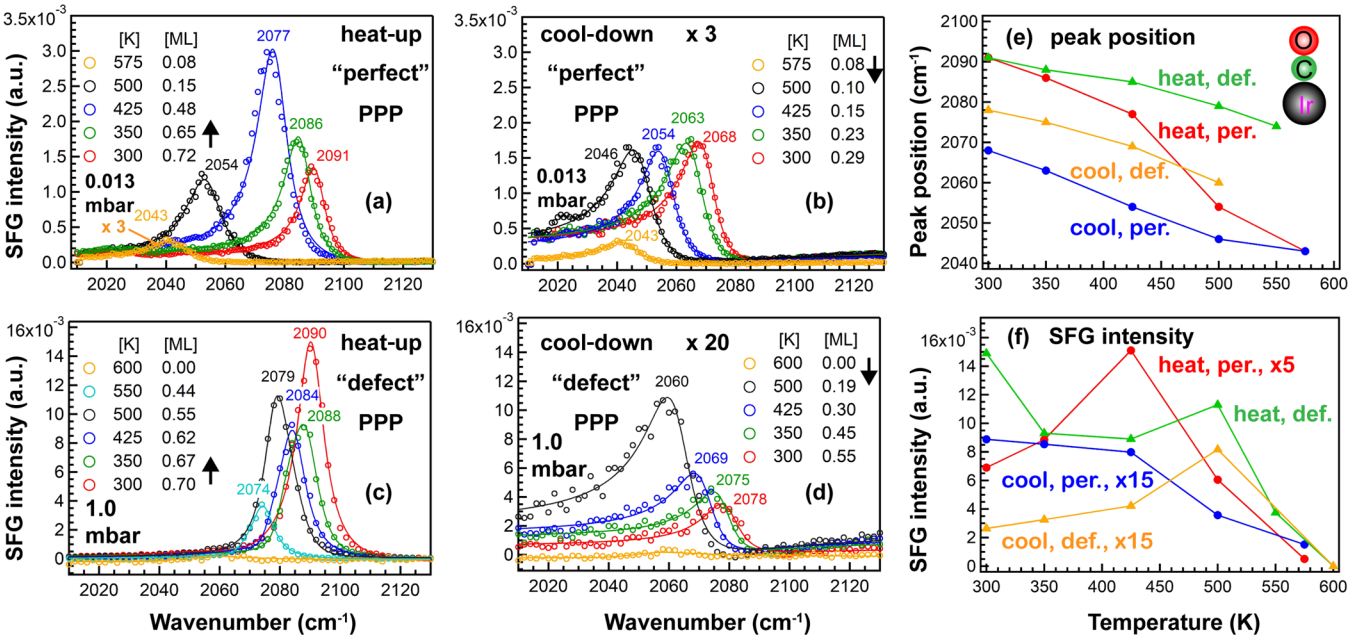

Figure 10. Temperature-dependent (300−600 K) SFG (PPP) spectra of CO on "perfect" (0.013 mbar) and "defect-rich" (1.0 mbar) Ir(111) upon stepwise heating (a,c) and subsequent stepwise cooling to 300 K (b,d). All PPP and SSP peak positions and spectral intensities of on-top CO as a function of temperature acquired upon heating and cooling are summarized in (e,f), respectively.

https://doi.org/10.1021/acs.jpcc.2c01141
J. Phys. Chem. C 2022, 126, 6578−6589

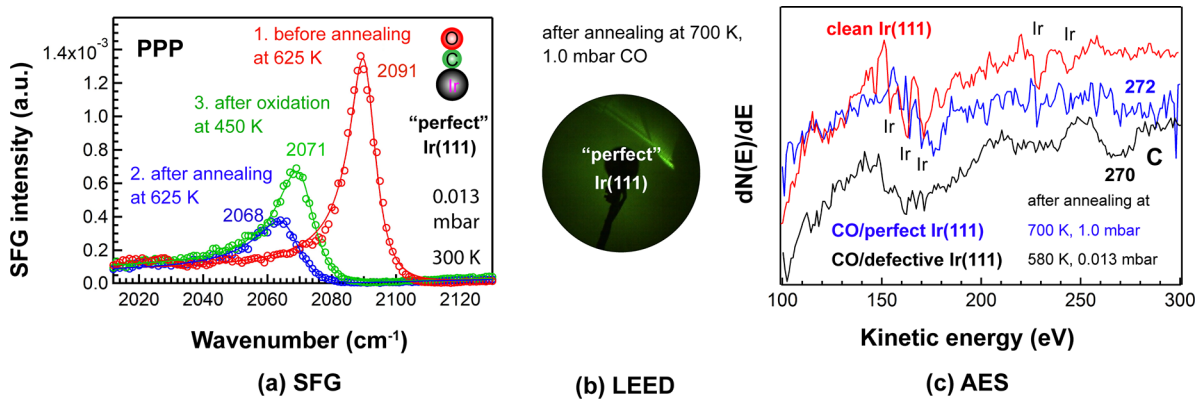

Figure 11. (a) Room-temperature PPP-SFG spectra of CO adsorption on "perfect" Ir(111) at 0.013 mbar, before (red) and after (blue) annealing at 625 K in CO, and after oxidation (green; 5×10^{-3} mbar O_2 at 450 K). (b) LEED pattern at E_0 = 87 eV acquired after exposing clean Ir(111) to 1.0 mbar CO at 300 K, heating in CO to 700 K for 60 min, and cooling to room temperature in UHV; (c) AES spectra at E_0 = 1500 eV.

herein, dissociation may occur at comparably lower temperature. CO may also dissociate on Ir adatoms or clusters mobilized by CO at high pressure, that is, CO-induced surface roughening, as observed for CO on Cu(100)[70] or Pt nanoparticles[71] at mbar CO pressure even around room temperature.

CO dissociation or disproportionation may thus be responsible for the irreversible changes that only occurred when heated higher than 570 K in (near) mbar CO pressure. The activation barriers of direct CO dissociation on noble metals were computed by DFT to be rather high,[28] but the barriers of CO disproportionation via the Boudouard reaction $2CO \leftrightarrow CO_2 + C$ on low-coordinated sites have been shown to be much lower (e.g., on Rh,[72] Cu,[73,74] or Pt[64]).

3.4.4. SFG, LEED, and AES Studies of Carbon Deposits. As seen in Figure 11a, after heating perfect Ir(111) to 625 K in 0.013 mbar CO, the room-temperature PPP spectrum of on-top CO originally centered at 2091 cm^{-1} (red) was red-shifted to 2068 cm^{-1} (blue), accompanied by a 3.5-fold intensity loss. To confirm that carbon was formed on the Ir(111) surface at 625 K, an oxidation experiment was then performed. As expected, after oxidation at 450 K in 5×10^{-3} mbar O_2, not only the peak position moved to higher wavenumbers (2071 vs 2068 cm^{-1}), but also the spectral intensity increased (green vs blue) because carbon was (partially) removed by oxidation. This "partly reversible" spectrum suggests that CO dissociation did occur at 625 K in 0.013 mbar of CO. Analogous to defect-rich Ir(111) (Figure 10c,d), a dissociation experiment was also carried out in 1.0 mbar CO (Figure 11b,c).

Carbon deposits increase the LEED background intensity and can be detected by AES,[19] while the dissociated oxygen is removed from the surface via reaction with gaseous CO. Accordingly, a LEED pattern was measured after dosing 1.0 mbar CO at 300 K and annealing at 700 K for 60 min in the high-pressure cell. As seen in Figure 11b, after cooling in UHV, the LEED pattern was fuzzy, indicating that the surface was covered by carbon. Subsequently, an AES spectrum was obtained (Figure 11c). Compared to the AES spectrum of clean Ir(111) (Figure 1b), apart from the Ir-peaks becoming weak, a broad carbon peak appeared centered at around 272 eV. The carbon peak was even stronger when the experiment was repeated in 0.013 mbar CO on "defective" Ir(111) (270 eV), suggesting that surface roughness is more crucial than CO pressure. Thus, CO dissociates on Ir(111) but clearly requires high pressure and high temperature. Carbon quantification by XPS, either in situ[64−66,75] or ex situ,[70] before/after high-pressure CO exposure is planned for the future.

3.5. DFT Study of CO Disproportionation. CO dissociation on Ir(111), still being rather unexpected, was further investigated computationally. DFT was used to study the disproportionation on Ir(111): $2CO \leftrightarrow CO_2 + C$.[49,50] The C and CO adsorption as well as the disproportionation of CO was modeled by 2 × 2 supercells of Ir(111) (using the theoretical equilibrium lattice parameter of 3.874 Å) with five layers of Ir (Figure 12). In good agreement with previous

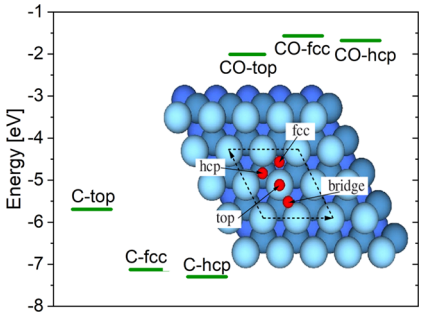

Figure 12. Adsorption energies of C and CO on Ir(111) at 0.25 ML coverage on various high-symmetry sites, which are indicated in the inset.

calculations,[24,27,28] a preference for CO adsorption on top sites and on hcp sites for C atoms was found (Table 1). The C

Table 1. Adsorption Energies (eV) of C and CO on Ir(111) at Various Sites and 0.25 ML Coverage[a]

site	top	fcc	hcp
C	−5.69	−7.13	**−7.30**
CO	**−2.01**	−1.57	−1.68

[a]The most stable sites are marked in bold.

adsorption is very strong, and C can be removed from the surface only under harsh oxygen-rich conditions. At larger coverages, however, also the hollow fcc or hcp sites can be occupied by CO, and overall, the binding energy of CO on Ir(111) gets reduced.[25]

In order to determine the dissociation barrier for CO, we put a second CO molecule on top but far away from the adsorbed CO (energy zero in Figure 13). Then, we used a

https://doi.org/10.1021/acs.jpcc.2c01141
J. Phys. Chem. C 2022, 126, 6578−6589

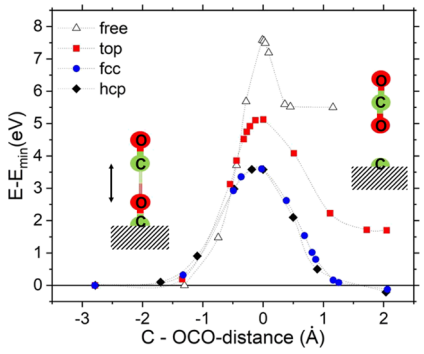

Figure 13. Energy barrier (in eV) for the Boudouard reaction $2CO \leftrightarrow C + CO_2$ in free space or with CO adsorbed on Ir(111) at three different sites. The energy zero is set to a large CO−CO distance (left side); the C−OCO distance (indicated by an arrow) is set to zero at the transition barrier. The lines are just guides to the eye.

constraint minimization technique, where the x and y coordinates of CO are fixed, but z of all atoms can relax. In addition, the C−OCO distance (see Figure 13) is automatically slowly reduced by an increasing pseudo force until the energy reaches a maximum and the pseudo forces change sign, which indicates the transition state. During this approach, the adsorbed CO molecule on the fcc or hcp site gets pushed deeper into the surface, increasing the Ir−C interaction and weakening the C−O bond. On the contrary, for the CO-top position, the Ir atom beneath CO acts like a hard wall and much less relaxation is possible. This leads to a relatively small activation energy of about 3.6 eV for the hcp and fcc sites (Figure 13), whereas more than 5.1 eV is necessary for the top position. However, this is still a drastic reduction compared to a reaction in free space with a barrier height of 7.6 eV. From Figure 13, it is also evident that the end products ($C + CO_2$) have unfavorable energies for the reaction in free space and on the Ir-top position (since C on top of Ir has the lowest C adsorption energy), whereas they are slightly favored for hcp/fcc sites since C is very strongly adsorbed there.

These computational results help to verify the experimental findings. At low coverage, CO adsorbs only at the top site and the activation energy is so high that CO would desorb from the surface before a disproportionation is possible. However, at high CO partial pressure and high CO surface coverage, the hcp/fcc sites are partially occupied, and with increasing temperature, the adsorbed CO molecule on these sites can react with gas-phase CO forming CO_2 and leaving a C atom behind, which remains strongly adsorbed and poisons the surface. CO adsorbed on hcp/fcc sites was experimentally not observed,[25] suggesting that it is a transient species in the process.

4. CONCLUSIONS

We have used surface-sensitive PD-SFG, LEED/AES, XPS, and DFT calculations to study CO adsorption and dissociation/disproportionation on both smooth and defect-rich Ir(111) surfaces. PD-SFG showed that, in contrast to the strong coverage dependence of the CO tilt angle on smooth Ir(111) (i.e., CO tilted 30° at 0.70 ML), on the defect-rich surface, CO preferred standing upright at high coverage (4° at 0.70 ML). When the coverage ranged from 0.67 to 0.55 ML on defective surfaces, the CO tilt angle remained constant at ∼10° but still rather small. CO forms three different overlayer structures as observed by LEED: $(\sqrt{3} \times \sqrt{3})R30°$ and $(2\sqrt{3} \times 2\sqrt{3})R30°$ at low CO exposure and $(3\sqrt{3} \times 3\sqrt{3})R30°$ at high CO exposure/pressure. XPS and LEED studies indicated that there is no CO dissociation at low pressure (10^{-6} mbar)/high temperature (890 K) or high pressure (1.0 mbar)/low temperature (500 K). However, upon heat-up (300 to ∼600 K) and cool-down (∼600 to 300 K) in a background of ∼1 mbar CO, the obtained irreversible SFG spectra implied that CO dissociated on smooth and especially defective Ir(111), yielding carbon deposits. SFG spectra upon carbon oxidation and AES spectra of Ir(111) after annealing in 1.0 mbar of CO at 700 K indirectly and directly confirmed the formation of surface carbon species, respectively. DFT calculations suggested that at high pressure, CO adsorbed on hcp/fcc sites can react with gas-phase CO via disproportionation, forming CO_2 and leaving a C atom behind on the Ir surface.

■ ASSOCIATED CONTENT

Supporting Information

The Supporting Information is available free of charge at https://pubs.acs.org/doi/10.1021/acs.jpcc.2c01141.

Evolution of LEED patterns of CO overlayer structures on Ir(111); PPP and SSP spectra of CO on "defect-rich" Ir(111); fitted results of pressure- and temperature-dependent PPP and SSP spectra of CO on "defect-rich" Ir(111); and fitted results of PPP spectra of CO on "perfect" and "defect-rich" Ir(111) (PDF)

■ AUTHOR INFORMATION

Corresponding Author

Günther Rupprechter − *Institute of Materials Chemistry, Technische Universität Wien, 1060 Vienna, Austria;* orcid.org/0000-0002-8040-1677; Phone: +43 (1) 58801-165100; Email: guenther.rupprechter@tuwien.ac.at

Authors

Xia Li − *Institute of Materials Chemistry, Technische Universität Wien, 1060 Vienna, Austria;* orcid.org/0000-0003-2504-239X

Thomas Haunold − *Institute of Materials Chemistry, Technische Universität Wien, 1060 Vienna, Austria*

Stefan Werkovits − *Institute of Materials Chemistry, Technische Universität Wien, 1060 Vienna, Austria*

Laurence D. Marks − *Department of Materials Science and Engineering, Northwestern University, Evanston, Illinois 60208, United States;* orcid.org/0000-0002-6659-2016

Peter Blaha − *Institute of Materials Chemistry, Technische Universität Wien, 1060 Vienna, Austria*

Complete contact information is available at: https://pubs.acs.org/10.1021/acs.jpcc.2c01141

Funding

Open Access is funded by the Austrian Science Fund (FWF).

Notes

The authors declare no competing financial interest.

■ ACKNOWLEDGMENTS

This work was supported by the Austrian Science Fund via projects M 2787-N (Lise Meitner Fellowship of XL: SFG spectroscopy of Pd/GR model catalysts) and I 4434-N (Single Atom Catalysis).

REFERENCES

(1) Küppers, J.; Plagge, A. Interaction of CO and O_2 with Ir(111) Surfaces. *J. Vac. Sci. Technol.* **1976**, *13*, 259−263.
(2) Wehner, S.; Baumann, F.; Küppers, J. Kinetic Hysteresis in the CO Oxidation Reaction on Ir(111) Surfaces. *Chem. Phys. Lett.* **2003**, *370*, 126−131.
(3) Corva, M.; Vesselli, E. Room Temperature Carbonylation of Iron-Phthalocyanines Adsorbed on a Single Crystal Metal Surface: An in Situ SFG Investigation at Near-Ambient Pressure. *J. Phys. Chem. C* **2016**, *120*, 22298−22303.
(4) Corva, M.; Feng, Z. J.; Dri, C.; Salvador, F.; Bertoch, P.; Comelli, G.; Vesselli, E. Carbon Dioxide Reduction on Ir(111): Stable Hydrocarbon Surface Species at Near-Ambient Pressure. *Phys. Chem. Chem. Phys.* **2016**, *18*, 6763−6772.
(5) da Silva, K. I. M.; Bernardi, F.; Abarca, G.; Baptista, D. L.; Santos, M. J. L.; Barquin, L. F.; Dupont, J.; de Pedro, I. Tuning the Structure and Magnetic Behavior of Ni-Ir-Based Nanoparticles in Ionic Liquids. *Phys. Chem. Chem. Phys.* **2018**, *20*, 10247−10257.
(6) Yang, T.; Wang, Y. H.; Wei, W. X.; Ding, X. R.; He, M. S.; Yu, T. T.; Zhao, H.; Zhang, D. E. Synthesis of Octahedral Pt-Ni-Ir Yolk-Shell Nanoparticles and Their Catalysis in Oxygen Reduction and Methanol Oxidization under Both Acidic and Alkaline Conditions. *Nanoscale* **2019**, *11*, 23206−23216.
(7) Sun, Y. J.; Huang, B. L.; Li, Y. J.; Xing, Y.; Luo, M. C.; Li, N.; Xia, Z. H.; Qin, Y. N.; Su, D.; Wang, L.; et al. Trifunctional Fishbone-Like PtCo/Ir Enables High-Performance Zinc-Air Batteries to Drive the Water-Splitting Catalysis. *Chem. Mater.* **2019**, *31*, 8136−8144.
(8) Inami, Y.; Ogihara, H.; Nagamatsu, S.; Asakura, K.; Yamanaka, I. Synergy of Ru and Ir in the Electrohydrogenation of Toluene to Methylcyclohexane on a Ketjenblack-Supported Ru-Ir Alloy Cathode. *ACS Catal.* **2019**, *9*, 2448−2457.
(9) Chen, K. K.; Guo, S.; Liu, H. Y.; Li, X. Y.; Zhang, Z. M.; Lu, T. B. Strong Visible-Light-Absorbing Cuprous Sensitizers for Dramatically Boosting Photocatalysis. *Angew. Chem., Int. Ed.* **2020**, *59*, 2−9.
(10) Zhang, J.; Chen, Z. L.; Liu, C.; Zhao, J.; Liu, S. L.; Rao, D. W.; Nie, A. M.; Chen, Y. N.; Deng, Y. D.; Hu, W. B. Hierarchical Iridium-Based Multimetallic Alloy with Double-Core-Shell Architecture for Efficient Overall Water Splitting. *Sci. China Mater.* **2020**, *63*, 249−257.
(11) Lang, E.; Müller, K.; Heinz, K.; Van Hove, M. A.; Koestner, R. J.; Somorjai, G. A. LEED Intensity Analysis of the (1 × 5) Reconstruction of Ir(100). *Surf. Sci.* **1983**, *127*, 347−365.
(12) Okwamoto, Y.; Bennemann, K. H. Theory for the Hexagonal Reconstruction of fcc(100) Surfaces of Metals. *Surf. Sci.* **1987**, *179*, 231−242.
(13) Ali, T.; Klötzer, B.; Walker, A. V.; King, D. A. A Molecular Beam Study of Nonlinearity in the CO-Induced Surface Restructuring of Ir{100}. *J. Chem. Phys.* **1998**, *109*, 10996.
(14) Somorjai, G. A.; Rupprechter, G. The Flexible Surface: Molecular Studies Explain the Extraordinary Diversity of Surface Chemical Properties. *J. Chem. Educ.* **1998**, *75*, 162−176.
(15) Anic, K.; Bukhtiyarov, A. V.; Li, H.; Rameshan, C.; Rupprechter, G. CO Adsorption on Reconstructed Ir(100) Surfaces from UHV to mbar Pressure: A LEED, TPD, and PM-IRAS Study. *J. Phys. Chem. C* **2016**, *120*, 10838−10848.
(16) Koch, R.; Borbonus, M.; Haase, O.; Rieder, K. H. New Aspects on the Ir(110) Reconstruction: Surface Stabilization on Mesoscopic Scale via (331) Facets. *Phys. Rev. Lett.* **1991**, *67*, 3416−3419.
(17) Grant, J. T. Some Studies on the Ir(111) Surface Using LEED and Auger Electron Spectroscopy. *Surf. Sci.* **1971**, *25*, 451−456.
(18) Hagen, G. I.; Nieuwenhuys, B. E.; Rovida, G.; Somorjai, G. A. Low-Energy Electron Diffraction, Auger Electron Spectroscopy, and Thermal Desorption Studies of Chemisorbed CO and O_2 on the (111) and Stepped [6(111) × (100)] Iridium Surfaces. *Surf. Sci.* **1976**, *57*, 632−650.
(19) Comrie, C. M.; Weinberg, W. H. Chemisorption of Carbon-Monoxide on Iridium (III) Surface. *J. Chem. Phys.* **1976**, *64*, 250−259.
(20) Lauterbach, J.; Boyle, R. W.; Schick, M.; Mitchell, W. J.; Meng, B.; Weinberg, W. H. The Adsorption of CO on Ir(111) Investigated with FT-IRAS. *Surf. Sci.* **1996**, *350*, 32−44.
(21) Zhang, V. L.; Arnolds, H.; King, D. A. Hot Band Excitation of CO/Ir{111} Studied by Broadband Sum Frequency Generation. *Surf. Sci.* **2005**, *587*, 102−109.
(22) Lane, I. M.; King, D. A.; Arnolds, H. The Determination of an Inhomogeneous Linewidth for a Strongly Coupled Adsorbate System. *J. Chem. Phys.* **2007**, *126*, No. 024707.
(23) Lane, I. M.; Liu, Z. P.; King, D. A.; Arnolds, H. Ultrafast Vibrational Dynamics of NO and CO Adsorbed on an Iridium Surface. *J. Phys. Chem. C* **2007**, *111*, 14198−14206.
(24) Noei, H.; Franz, D.; Creutzburg, M.; Müller, P.; Krausert, K.; Grånäs, E.; Taube, R.; Mittendorfer, F.; Stierle, A. Monitoring the Interaction of CO with Graphene Supported Ir Clusters by Vibrational Spectroscopy and Density Functional Theory Calculations. *J. Phys. Chem. C* **2018**, *122*, 4281−4289.
(25) Li, X.; Pramhaas, V.; Rameshan, C.; Blaha, P.; Rupprechter, G. Coverage-Induced Orientation Change: CO on Ir(111) Monitored by Polarization-Dependent Sum Frequency Generation Spectroscopy and Density Functional Theory. *J. Phys. Chem. C* **2020**, *124*, 18102−18111.
(26) Baronio, S.; Leo, V. D.; Lautizi, G.; Mantegazza, P.; Natale, E.; Tuniz, M.; Vigneri, S.; Bignardi, L.; Lacovig, P.; Lizzit, S.; et al. Vibrational Fine Structure in C 1s High-Resolution Core-Level Spectra of CO Chemisorbed on Ir(111). *J. Phys. Chem. C* **2022**, *126*, 1411−1419.
(27) Krekelberg, W. P.; Greeley, J.; Mavrikakis, M. Atomic and Molecular Adsorption on Ir(111). *J. Phys. Chem. B* **2004**, *108*, 987−994.
(28) Liu, C. L.; Zhu, L.; Ren, P. J.; Wen, X. D.; Li, Y. W.; Jiao, H. J. High-Coverage CO Adsorption and Dissociation on Ir(111), Ir(100), and Ir(110) from Computations. *J. Phys. Chem. C* **2019**, *123*, 6487−6495.
(29) Bourguignon, B.; Carrez, S.; Dragnea, B.; Dubost, H. Vibrational Spectroscopy of Imperfect CO/Pd(111) Surfaces Obtained by Adsorption between 150 and 230 K. *Surf. Sci.* **1998**, *418*, 171−180.
(30) Rupprechter, G.; Freund, H.-J. Adsorbate-Induced Restructuring and Pressure-Dependent Adsorption on Metal Nanoparticles Studied by Electron Microscopy and Sum Frequency Generation Spectroscopy. *Top. Catal.* **2001**, *14*, 3−14.
(31) Unterhalt, H.; Rupprechter, G.; Freund, H.-J. Vibrational Sum Frequency Spectroscopy on Pd(111) and Supported Pd Nanoparticles: CO Adsorption from Ultrahigh Vacuum to Atmospheric Pressure. *J. Phys. Chem. B* **2002**, *106*, 356−367.
(32) Rupprechter, G. 8 surface Vibrational Spectroscopy on Noble Metal Catalysts from Ultrahigh Vacuum to Atmospheric Pressure. *Annu. Rep. Prog. Chem., Sect. C: Phys. Chem.* **2004**, *100*, 237−311.
(33) Shen, Y. R. Surface-Properties Probed by 2nd-Harmonic and Sum-Frequency Generation. *Nature* **1989**, *337*, 519−525.
(34) Zhuang, X.; Miranda, P. B.; Kim, D.; Shen, Y. R. Mapping Molecular Orientation and Conformation at Interfaces by Surface Nonlinear Optics. *Phys. Rev. B* **1999**, *59*, 12632−12640.
(35) Galletto, P.; Unterhalt, H.; Rupprechter, G. The Molecular Orientation of CO on Pd(111): A Polarization-Dependent SFG Study. *Chem. Phys. Lett.* **2003**, *367*, 785−790.
(36) Wang, H. F.; Gan, W.; Lu, R.; Rao, Y.; Wu, B. H. Quantitative Spectral and Orientational Analysis in Surface Sum Frequency Generation Vibrational Spectroscopy (SFG-VS). *Int. Rev. Phys. Chem.* **2005**, *24*, 191−256.
(37) Liu, W. T.; Zhang, L. N.; Shen, Y. R. Interfacial Structures of Methanol: Water Mixtures at a Hydrophobic Interface Probed by Sum-Frequency Vibrational Spectroscopy. *J. Chem. Phys.* **2006**, *125*, 144711.
(38) Li, X.; Deng, G. H.; Feng, R. J.; Lin, K.; Zhang, Z.; Bai, Y.; Lu, Z.; Guo, Y. Salt Effect on Molecular Orientation at Air/Liquid Methanol Interface. *Chin. Chem. Lett.* **2016**, *27*, 535−539.

https://doi.org/10.1021/acs.jpcc.2c01141
J. Phys. Chem. C 2022, 126, 6578−6589

(39) Li, X.; Roiaz, M.; Pramhaas, V.; Rameshan, C.; Rupprechter, G. Polarization-Dependent SFG Spectroscopy of Near Ambient Pressure CO Adsorption on Pt(111) and Pd(111) Revisited. *Top. Catal.* **2018**, *61*, 751−762.
(40) Li, X.; Rupprechter, G. A Modeling Analysis of Molecular Orientation at Interfaces by Polarization-Dependent Sum Frequency Generation Vibrational Spectroscopy. *Chin. J. Catal.* **2019**, *40*, 1655−1667.
(41) Hirose, C.; Akamatsu, N.; Domen, K. Formulas for the Analysis of the Surface SFG Spectrum and Transformation Coefficients of Cartesian SFG Tensor Components. *Appl. Spectrosc.* **1992**, *46*, 1051−1072.
(42) Li, X.; Rupprechter, G. Sum Frequency Generation Spectroscopy in Heterogeneous Model Catalysis: A Minireview of CO-Related Processes. *Catal. Sci. Technol.* **2021**, *11*, 12−26.
(43) Roiaz, M.; Pramhaas, V.; Li, X.; Rameshan, C.; Rupprechter, G. Atmospheric Pressure Reaction Cell for Operando Sum Frequency Generation Spectroscopy of Ultrahigh Vacuum Grown Model Catalysts. *Rev. Sci. Instrum.* **2018**, *89*, No. 045104.
(44) Grånäs, E.; Andersen, M.; Arman, M. A.; Gerber, T.; Hammer, B.; Schnadt, J.; Andersen, J. N.; Michely, T.; Knudsen, J. CO Intercalation of Graphene on Ir(111) in the Millibar Regime. *J. Phys. Chem. C* **2013**, *117*, 16438−16447.
(45) Corva, M.; Ferrari, A.; Rinaldi, M.; Feng, Z.; Roiaz, M.; Rameshan, C.; Rupprechter, G.; Costantini, R.; Dell'Angela, M.; Pastore, G.; et al. Vibrational Fingerprint of Localized Excitons in a Two-Dimensional Metal-Organic Crystal. *Nat. Commun.* **2018**, *9*, 4703.
(46) Vogel, D.; Spiel, C.; Schmid, M.; Stöger-Pollach, M.; Schlögl, R.; Suchorski, Y.; Rupprechter, G. The Role of Defects in the Local Reaction Kinetics of CO Oxidation on Low-Index Pd Surfaces. *J. Phys. Chem. C* **2013**, *117*, 12054−12060.
(47) Rupprechter, G. Sum Frequency Generation and Polarization−Modulation Infrared Reflection Absorption Spectroscopy of Functioning Model Catalysts from Ultrahigh Vacuum to Ambient Pressure. In *Adv. Catal.*, Gates, B. C., Knözinger, H., Eds.; Academic: New York, 2007; Vol. *51*, pp 133−263.
(48) Haunold, T.; Rupprechter, G. LiOx-Modification of Ni and Co_3O_4 Surfaces: An XPS, LEIS and LEED Study. *Surf. Sci.* **2021**, *713*, No. 121915.
(49) Blaha, P.; Schwarz, K.; Madsen, G. K. H.; Kvasnicka, D.; Luitz, J.; Laskowski, R.; Tran, F.; Marks, L. D. *WIEN2k: An Augmented Plane Wave Plus Local Orbitals Program for Calculating Crystal Properties*; Vienna University of Technology: Austria, 2018.
(50) Blaha, P.; Schwarz, K.; Tran, F.; Laskowski, R.; Madsen, G. K. H.; Marks, L. D. WIEN2k: An APW+lo Program for Calculating the Properties of Solids. *J. Chem. Phys.* **2020**, *152*, No. 074101.
(51) Perdew, J. P.; Burke, K.; Ernzerhof, M. Generalized Gradient Approximation Made Simple. *Phys. Rev. Lett.* **1996**, *77*, 3865−3868.
(52) Perdew, J. P.; Burke, K.; Ernzerhof, M. Generalized Gradient Approximation Made Simple (Vol 77, Pg 3865, 1996). *Phys. Rev. Lett.* **1997**, *78*, 1396−1396.
(53) Gleissner, R.; Creutzburg, M.; Noei, H.; Stierle, A. Interaction of Water with Graphene/Ir(111) Studied by Vibrational Spectroscopy. *Langmuir* **2019**, *35*, 11285−11290.
(54) Yang, L.-M.; Yau, S.-L. The Structures of Iodine and Carbon Monoxide Overlayers on Ir(111) Electrodes: An in Situ Scanning Tunneling Microscopy Study. *J. Phys. Chem. B* **2000**, *104*, 1769−1776.
(55) Su, X. C.; Cremer, P. S.; Shen, Y. R.; Somorjai, G. A. Pressure Dependence (10^{-10}−700 Torr) of the Vibrational Spectra of Adsorbed CO on Pt(111) Studied by Sum Frequency Generation. *Phys. Rev. Lett.* **1996**, *77*, 3858−3860.
(56) Crossley, A.; King, D. A. Infrared-Spectra for CO Isotopes Chemisorbed on Pt{111}: Evidence for Strong Absorbate Coupling Interactions. *Surf. Sci.* **1977**, *68*, 528−538.
(57) Symonds, J. P. R.; Arnolds, H.; Zhang, V. L.; Fukutani, K.; King, D. A. Broadband Femtosecond Sum-Frequency Spectroscopy of CO on Ru{1010} in the Frequency and Time Domains. *J. Chem. Phys.* **2004**, *120*, 7158−7164.
(58) Hayden, B. E.; Kretzschmar, K.; Bradshaw, A. M.; Greenler, R. G. An Infrared Study of the Adsorption of CO on a Stepped Platinum Surface. *Surf. Sci.* **1985**, *149*, 394−406.
(59) Greenler, R. G.; Burch, K. D.; Kretzschmar, K.; Klauser, R.; Bradshaw, A. M.; Hayden, B. E. Stepped Single-Crystal Surfaces as Models for Small Catalyst Particles. *Surf. Sci.* **1985**, *152*, 338−345.
(60) Luo, T.; Zhang, R. D.; Peng, X. X.; Liu, X. T.; Zhou, C. Y.; Yang, X. M.; Ren, Z. F. A Broadband Sum-Frequency Generation Vibrational Spectrometer to Probe Adsorbed Molecules on Nanoparticles. *Surf. Sci.* **2019**, *689*, No. 121459.
(61) Zhdan, P. A.; Boreskov, G. K.; Boronin, A. I.; Schepelin, A. P.; Egelhoff, W. F., Jr.; Weinberg, W. H. The Chemisorption of Carbon Monoxide on Iridium and Platinum Studied by UV- and X-ray Photoelectron Spectroscopy. *Surf. Sci.* **1978**, *71*, 267−278.
(62) Kung, K. Y.; Chen, P.; Wei, F.; Shen, Y. R.; Somorjai, G. A. Sum-Frequency Generation Spectroscopic Study of CO Adsorption and Dissociation on Pt(111) at High Pressure and Temperature. *Surf. Sci.* **2000**, *463*, L627−L633.
(63) Kung, K. Y.; Chen, P.; Wei, F.; Rupprechter, G.; Shen, Y. R.; Somorjai, G. A. Ultrahigh Vacuum High-Pressure Reaction System for 2-Infrared 1-Visible Sum Frequency Generation Studies. *Rev. Sci. Instrum.* **2001**, *72*, 1806−1809.
(64) Pramhaas, V.; Roiaz, M.; Bosio, N.; Corva, M.; Rameshan, C.; Vesselli, E.; Grönbeck, H.; Rupprechter, G. Interplay between CO Disproportionation and Oxidation: On the Origin of the CO Reaction Onset on Atomic Layer Deposition-Grown Pt/ZrO_2 Model Catalysts. *ACS Catal.* **2021**, *11*, 208−214.
(65) Kaichev, V. V.; Morkel, M.; Unterhalt, H.; Prosvirin, I. P.; Bukhtiyarov, V. I.; Rupprechter, G.; Freund, H.-J. C−O Bond Scission on "Defect-Rich and Perfect" Pd(111)? *Surf. Sci.* **2004**, *566*−*568*, 1024−1029.
(66) Rupprechter, G.; Kaichev, V. V.; Unterhalt, H.; Morkel, M.; Bukhtiyarov, V. I. CO Dissociation and CO Hydrogenation on Smooth and Ion-Bombarded Pd(111): SFG and XPS Spectroscopy at mbar Pressures. *Appl. Surf. Sci.* **2004**, *235*, 26−31.
(67) Rodríguez de la Fuente, O.; Borasio, M.; Galletto, P.; Rupprechter, G.; Freund, H.-J. The Influence of Surface Defects on Methanol Decomposition on Pd(111) Studied by XPS and PM-IRAS. *Surf. Sci.* **2004**, *566*−*568*, 740−745.
(68) Mehmood, F.; Stolbov, S.; Rahman, T. S. C and S Induce Changes in the Electronic and Geometric Structure of Pd(533) and Pd(320). *J. Phys.: Condens. Matter* **2006**, *18*, 8015−8027.
(69) Stolbov, S.; Mehmood, F.; Rahman, T. S.; Alatalo, M.; Makkonen, I.; Salo, P. Site Selectivity in Chemisorption of C on Pd(211). *Phys. Rev. B* **2004**, *70*, No. 155410.
(70) Roiaz, M.; Falivene, L.; Rameshan, C.; Cavallo, L.; Kozlov, S. M.; Rupprechter, G. Roughening of Copper (100) at Elevated CO Pressure: Cu Adatom and Cluster Formation Enable CO Dissociation. *J. Phys. Chem. C* **2019**, *123*, 8112−8121.
(71) Haghofer, A.; Sonström, P.; Fenske, D.; Föttinger, K.; Schwarz, S.; Bernardi, J.; Al-Shamery, K.; Bäumer, M.; Rupprechter, G. Colloidally Prepared Pt Nanowires Versus Impregnated Pt Nanoparticles: Comparison of Adsorption and Reaction Properties. *Langmuir* **2010**, *26*, 16330−16338.
(72) Pery, T.; Schweitzer, M. G.; Volpp, H. R.; Wolfrum, J.; Ciossu, L.; Deutschmann, O.; Warnatz, J. Sum-Frequency Generation in Situ Study of CO Adsorption and Catalytic CO Oxidation on Rhodium at Elevated Pressures. *Proc. Combust. Inst.* **2002**, *29*, 973−980.
(73) Olmos-Asar, J. A.; Monachino, E.; Dri, C.; Peronio, A.; Africh, C.; Lacovig, P.; Comelli, G.; Baldereschi, A.; Peressi, M.; Vesselli, E. CO on Supported Cu Nanoclusters: Coverage and Finite Size Contributions to the Formation of Carbide via the Boudouard Process. *ACS Catal.* **2015**, *5*, 2719−2726.
(74) Ng, M. L.; Abild-Pedersen, F.; Kaya, S.; Mbuga, F.; Ogasawara, H.; Nilsson, A. Low Barrier Carbon Induced CO Dissociation on Stepped Cu. *Phys. Rev. Lett.* **2015**, *114*, No. 246101.

https://doi.org/10.1021/acs.jpcc.2c01141
J. Phys. Chem. C 2022, 126, 6578−6589

(75) Rupprechter, G. Operando Surface Spectroscopy and Microscopy During Catalytic Reactions: From Clusters via Nanoparticles to Meso-Scale Aggregates. *Small* **2021**, *17*, No. 2004289.

https://doi.org/10.1021/acs.jpcc.2c01141
J. Phys. Chem. C 2022, 126, 6578−6589